Colloidal Synthesis of Air-Stable Alloyed $CsSn_{1-x}Pb_xI_3$ Perovskite Nanocrystals for Use in Solar Cells

Feng Liu,[1] Chao Ding,[1] Yaohong Zhang,[1] Teresa S. Ripolles,[2] Taichi Kamisaka,[1] Taro Toyoda,[1,8] Shuzi Hayase,*[,2,8] Takashi Minemoto,[3,8] Kenji Yoshino,[4,8] Songyuan Dai,[5] Masatoshi Yanagida,[6,7] Hidenori Noguchi,[6,7] and Qing Shen*[,1,8]

[1]Faculty of Informatics and Engineering, The University of Electro-Communications, 1-5-1 Chofugaoka, Chofu, Tokyo 182-8585, Japan

[2]Faculty of Life Science and Systems Engineering, Kyushu Institute of Technology, 2-4 Hibikino, Wakamatsu-ku, Kitakyushu, Fukuoka 808-0196, Japan

[3]Department of Electrical and Electronic Engineering, Faculty of Science and Engineering, Ritsumeikan University, 1-1-1 Nojihigashi, Kusatsu, Shiga 525-8577, Japan

[4]Department of Electrical and Electronic Engineering, Miyazaki University, 1-1 Gakuen, Kibanadai Nishi, Miyazaki 889-2192, Japan

[5]Beijing Key Laboratory of Novel Thin Film Solar Cells, State Key Laboratory of Alternate Electrical Power System with Renewable Energy Sources, North China Electric Power University, Beijing 102206, P. R. China

[6]Center for Green Research on Energy and Environmental Materials, National Institute for Materials Science (NIMS), Tsukuba 305-0044, Japan

[7]Global Research Center for Environmental and Energy based on Nanomaterials Science, National Institute for Materials Science (NIMS), Tsukuba 305-0044, Japan

[8]CREST, Japan Science and Technology Agency (JST), 4-1-8 Honcho, Kawaguchi, Saitama 332-0012, Japan

E-mail: shen@pc.uec.ac.jp, hayase@life.kyutech.ac.jp

Abstract

Organic-inorganic hybrid perovskite solar cells have demonstrated unprecedented high power conversion efficiencies in the past few years. Now, the universal instability of the perovskites has become the main barrier for this kind of solar cells to

realize commercialization. This situation can be even worse for those tin-based perovskites, especially for $CsSnI_3$, because upon exposure to ambient atmosphere the desired black orthorhombic phase $CsSnI_3$ would promptly lose single crystallinity and degrade to the inactive yellow phase, followed by irreversible oxidation into metallic Cs_2SnI_6. By alloying $CsSnI_3$ with $CsPbI_3$, we herein report the synthesis of alloyed perovskite quantum dot (QD), $CsSn_{1-x}Pb_xI_3$, which not only can be phase-stable for months in purified colloidal solution but also remains intact even directly exposed to ambient air, far superior to both of its parent $CsSnI_3$ and $CsPbI_3$ QDs. Ultrafast transient absorption spectroscopy studies reveal that the photoexcited electrons in the alloyed QDs can be injected into TiO_2 nanocrystals at a fast rate of 1.12×10^{11} s^{-1}, which enables a high photocurrent generation in solar cells.

Keywords: all-inorganic perovskite, stable tin perovskite, colloidal perovskite nanocrystals, alloyed tin/lead perovskite, ultrafast exciton dynamics

Introduction

Solution-processable halide perovskite materials have gained broader interest in recent years due to their numerous potential applications, including high-efficiency photovoltaic cells, light-emitting diodes, photo-detectors, and lasers.[1-5] While recent studies have been mostly focused on organic-inorganic hybrid compounds, such as ABX_3 (A = $CH_3NH_3^+$ and $CH_3(NH_2)_2^+$, B = Pb^{2+}, Sn^{2+}, Cu^{2+}, Bi^{3+}, and Sb^{3+}, X = Cl^-, Br^-, and I^-), the studies of their inorganic analogues, like $CsBX_3$, are not as advanced.[6-9] In fact, compared to those organic-inorganic hybrid perovskites, all-inorganic Cs-based compounds were demonstrated to possess higher compositional stability under environmental stresses (*e.g.*, heat and humidity).[1,10,11] One such example is $CsPbI_3$, which stands out as a promising optoelectronic material with the additional advantages of low defect density, high photoluminescence (PL) quantum yield, and long carrier diffusion length.[10,12-14] More recently, an inspiring high power conversion efficiency of 10.77% was achieved for thin film solar cells

based on $CsPbI_3$ quantum dots (QDs), which has surpassed most other QD solar cell technologies.[1] However, in addition to the general toxicity issues that encountered by these all-lead perovskites, $CsPbI_3$ QDs still suffer from phase-related stability problems as its desired red cubic phase (B-α) spontaneously transforms to the inactive orthorhombic phase when they are processed into solid thin films and directly exposed to open air.[1] What's more, although $CsPbI_3$ has a narrower band gap (~1.73 eV in the bulk) when compared with $CsPbBr_3$ (~2.25 eV) and $CsPbCl_3$ (~3.05 eV), it is still non-ideal and their near-infrared application is limited.[13] Besides, in the form of nanostructures, the band gap of $CsPbI_3$ would become larger due to the quantum confinement effects, typically ranging from 1.85 to 1.97 eV.[10,15] In view of the above, it is highly encouraged to find alternatives being more stable, lower in lead content, and possessing wide spectral response.[16-18] All-inorganic lead-free perovskite $CsSnI_3$ is such a potential candidate, which is a direct-gap semiconductor with band gap of 1.3 eV (in bulk) and small exciton binding energy. It exhibits strong absorption over the visible to near infrared region, and would thus enable a higher light harvesting efficiency in photovoltaics.[19,20] $CsSnI_3$ has also been demonstrated to be an efficient hole transport material in dye-sensitized solar cells owing to their remarkable hole mobility of ~585 $cm^2\ V^{-1}\ s^{-1}$.[21,22] In fact, Sn-based perovskite has been now a frontier of perovskite research and holds great potential for use in various applications.[23] However, from the aspect of phase stability and practical deployment, $CsSnI_3$ is even more susceptible than $CsPbI_3$ because of its higher sensitivity to air, moisture, and even non-polar organic solvents.[20,21,24] It is observed that upon direct exposure to air the prepared active black orthorhombic phase (B-γ) $CsSnI_3$ would promptly lose single crystallinity, rapidly degrade to the inactive yellow polymorph, and ultimately oxidized into metallic Cs_2SnI_6.[21,24-26] In the last few years, significant efforts have been devoted to improve the phase stability of these Sn-based perovskites. For example, Sum *et al.* and Falaras *et al.* found that the SnF_2-doped $CsSnI_3$ possesses higher chemical stability than the pure material.[27,28] Further, Hatton and co-workers studied a series of tin halide additives including SnF_2, $SnCl_2$, $SnBr_2$, and SnI_2. They found that incorporating $CsSnI_3$ with $SnCl_2$ would be more effective in improving

their resistance to ambient air.[25] However, stability of these resulting doped $CsSnI_3$ is still not satisfactory as they could only survive about 3 h exposure to open air.[25] Therefore, stability of the Sn-based perovskites still needs to be further improved, yet it remains challenging for the perovskite community.

In this study, we report the alloyed Sn/Pb perovskite nanocrystals, $CsSn_{1-x}Pb_xI_3$ QDs, which not only can be phase-stable for months in purified colloidal solution but also remain intact even directly exposed to ambient air, far superior to both of its parent $CsSnI_3$ and $CsPbI_3$ QDs. In fact, previous studies on traditional alloyed nanomaterials such as $CdSe_xTe_{1-x}$, $Zn_xCd_{1-x}Se$, and $InAs_xP_{1-x}$ have revealed that alloying of two semiconductors at the nanometer scale would produce materials that display properties distinct not only from the properties of the bulk counterparts but also from those of their parent nanocrystals.[29-32] In recent case of perovskites, the alloying strategy using mixed cations and halides has also resulted in those alloyed perovskites with enhanced stability and physicochemical properties when compared to their parent compounds.[33-36] Herein, we show that both the susceptible Sn and Pb perovskites can also benefit from such alloying strategy. First, by combining $CsSnI_3$ and $CsPbI_3$, the as-synthesized $CsSn_xPb_{1-x}I_3$ QDs can be readily extracted from the crude solution through a facile antisolvent washing process using methyl acetate (MeOAc), which is essential to remove those remaining organic impurities for further characterization and use. This finding is also of particular importance since it has been challenging to extract the synthesized B-γ $CsSnI_3$ QDs as they degrade immediately once such antisolvent is added. Further, the resulting purified $CsSn_xPb_{1-x}I_3$ QDs exhibit extraordinary phase stability whether stored in solution or directly exposed to ambient air, paving the way for their practical use in various fields. As an example of their potential deployment in solar cells, we carried out ultrafast transient absorption (TA) spectroscopy studies to investigate the exciton dynamics within these QDs, which reveal that the photoexcited electrons in the alloyed QDs can transfer to the nanocrystalline TiO_2 within a fast rate of 1.12×10^{11} s^{-1}, enabling a high photocurrent generation in solar cells. The implications of these results for solar energy conversion will be discussed.

Results and discussion

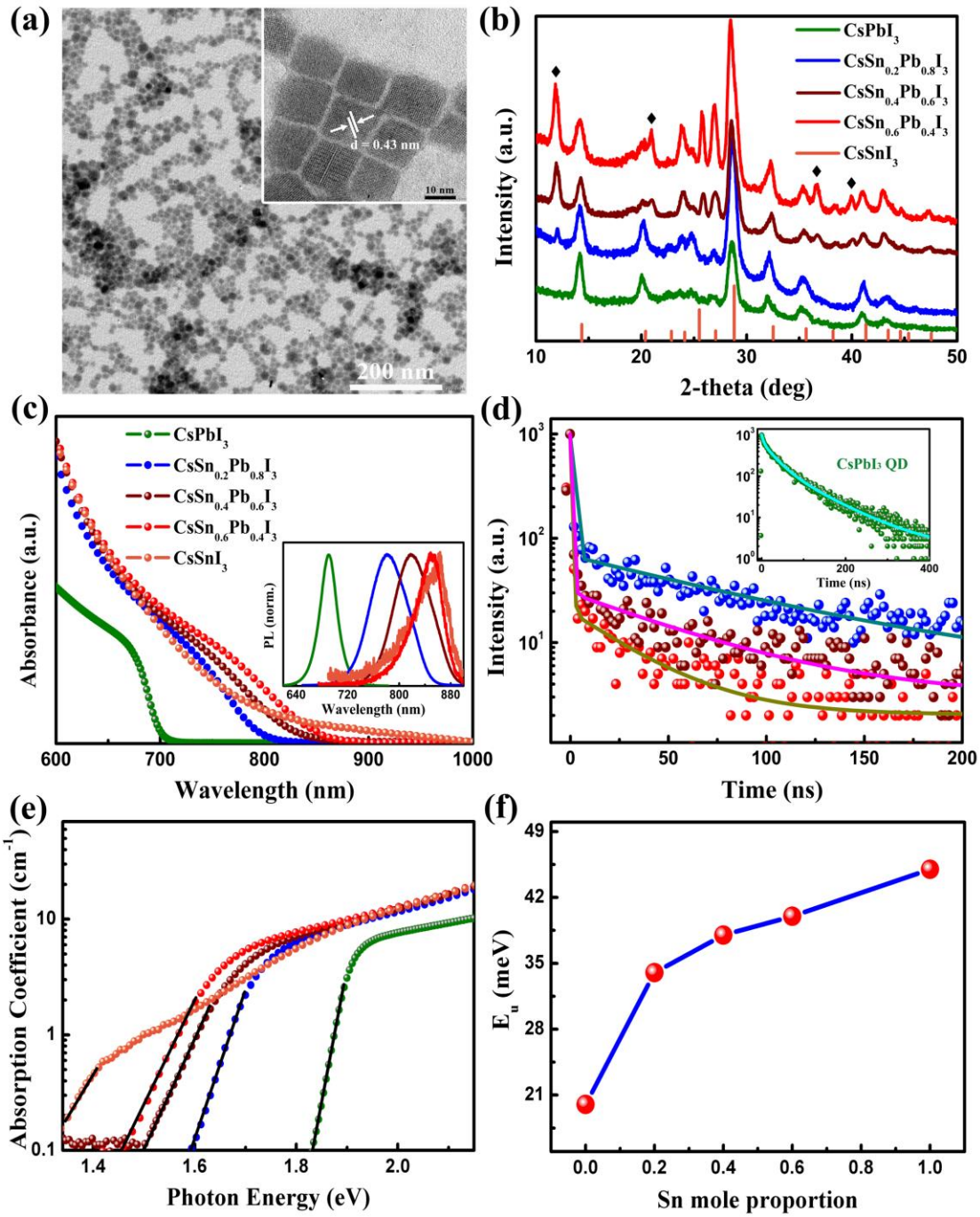

Figure 1. (a) TEM image of the purified $CsSn_{0.6}Pb_{0.4}I_3$ QDs synthesized at 160 °C. (b) XRD patterns of the $CsSn_{1-x}Pb_xI_3$ QDs with different stoichiometries. The position of each electron diffraction peak for $CsSnI_3$ was derived from References **21**, **28**, and **37**. (c) UV-vis absorption spectra of the alloyed QDs prepared at 160 °C with various stoichiometries. The inset shows their corresponding normalized steady-state PL

spectra. Note that $CsSnI_3$ QD solution prepared for UV-vis absorption measurement is crude solution diluted by hexane and measured within 1 min after synthesis. (d) Time-resolved PL decays for all samples in **(c)** except $CsSnI_3$. Excitation intensity and wavelength are 0.9 $\mu J/cm^2$ and 532 nm, respectively. Solid lines: fits to bi-exponential decay functions. (e) Optical absorption spectra of the alloyed QDs. (f) Urbach energies calculated for all samples in **(e)** as a function of Sn mole proportion.

The alloyed perovskite $CsSn_{1-x}Pb_xI_3$ QDs were prepared under nitrogen using standard Schlenk line technique, where SnI_2/PbI_2 mixture dissolved in trioctylphosphine was rapidly (<1 s) injected into an octadecene solution containing Cs precursor at 120-170 °C. Purification of the as-synthesized QDs was carried out according to a recently developed washing process using antisolvent MeOAc (see Supporting Information for more experimental details).[1] It is important to note that a molar ratio of $PbI_2/SnI_2 > 0.1$ in the injected Pb/Sn precursor is required to yield QDs with tolerance to MeOAc washing, otherwise, just like the pure $CsSnI_3$ QDs, they will degrade immediately once antisolvent MeOAc is added. ^{1}H nuclear magnetic resonance (NMR) measurement shown in Figure S1 confirms the efficacy of MeOAc washing, where resonance contributions from those excess organics, such as octadecene, oleic acid, oleylamine, and trioctylphosphine, are significantly reduced after two times of MeOAc washing, indicative of the removal of these organics from QD solution. Figure 1a shows a representative high-resolution TEM image of the purified sample, where uniform cubic-shaped dots with well-resolved lattice fringes can be clearly identified, indicating highly crystalline structure of the resulting QDs. Particle size of the as-synthesized QDs can be tuned from 11~14 nm by the choice of injection temperature from 120 to 170 °C as shown in Figure S2. However, it has to be pointed out that QDs prepared below 140 °C have a wide size distribution, only those synthesized above 140 °C feature a high uniformity in both size and shape (size distribution diagram of these various different QDs can be found in Figure S2). Also, we note that above 160 °C, particle size and shape of the resulting QDs do not change significantly but instead we can see black precipitates formed at the bottom of the

flask, which are identified to be bulk $CsSn_{1-x}Pb_xI_3$. Taking $CsSn_{0.6}Pb_{0.4}I_3$ QD as an example, UV-vis absorption spectra of the different-sized QDs are shown in Figure S3. It is seen that the optical absorption band edge of the resulting $CsSn_{0.6}Pb_{0.4}I_3$ QDs only slightly red-shifts from 830 to 850 nm with increasing particle size, indicating a weak quantum confinement in our large-sized QDs. It is also worth mentioning that at a given reaction temperature, varying the molar ratio of the starting materials of PbI_2 and SnI_2 in the Pb/Sn precursor solution does not much affect the final size of the QDs, while their chemical composition is significantly changed. Atomic ratio of Pb/Sn (*i.e.*, x/1-x) in the resulting $CsSn_{1-x}Pb_xI_3$ QDs is strongly dependent on the dose of the precursors of PbI_2 and SnI_2, and can be facilely tuned from ~4 to 0.6 with the adjustment of the PbI_2 amount, which is determined by elemental analysis *via* X-ray photoelectron spectroscopy (XPS, Figure S4) measurement. Table S1 summarizes the detailed synthetic conditions for obtaining various different alloyed QDs.

X-ray diffraction (XRD) spectra of the alloyed QDs with different stoichiometries are shown in Figure 1b. For carrying out XRD measurements, QD solid samples were prepared by depositing purified QD hexane solution onto a glass substrate and then dried by spin-casting at 1000 rpm for 20 s. For reference B-γ $CsSnI_3$ QDs, the positions of diffraction peaks were taken from previous reports on bulk semiconductor because during the essential QD extraction after synthesis the B-γ $CsSnI_3$ QDs degrade promptly upon the addition of normal polar solvents like MeOAc, butanol, and acetone, *etc*. or even just diluted with common non-polar solvents (*e.g.*, hexane, toluene, and octane). Thus, it is difficult to isolate the desired black-phase $CsSnI_3$ QDs, let alone to prepare their solid films or powders for XRD measurement. In Figure 1b, XRD spectra of the alloyed QDs were compared to that of the pure $CsPbI_3$ QDs and bulk $CsSnI_3$. It is shown that the diffraction peaks of the alloyed QDs at 23.8°, 25.7° and 27.0° gradually increase in intensity with the increase of Sn/Pb atomic ratio, which is also followed by the appearance of new sharp peaks at 39.8°, 36.6°, 20.8° and 11.7° (indicated with cubes). We rule out the possibility that these new diffraction peaks come from impurities such as PbI_2, CsI, SnI_2/SnI_4, or their mixtures because XRD patterns of these inorganic salts do not match with these

observed positions (Figure S5). The appearance of the new diffraction peaks that are different from parent $CsSnI_3$ or $CsPbI_3$ thus indicates that our alloyed QDs adopt a different crystal structure (as discussed later).

UV-vis absorption and normalized PL spectra of the alloyed QDs with different stoichiometries are shown in Figure 1c. By making use of the merit of Sn, we can now see the optical absorption band edge of the alloyed QDs extends to the near-infrared region of ~850 nm, superior to that of the pure $CsPbI_3$ QDs at ~700 nm. In addition, an obvious red shift in both absorption and PL spectra is observed with increasing Sn content. This is no surprise that band gap of $CsSnI_3$ is narrower than that of $CsPbI_3$. The continuous absorption and PL spectra shifting of the alloyed QDs also rules out phase separation or separated nucleation of $CsSnI_3$ or $CsPbI_3$ QDs. Because if $CsSnI_3$ or $CsPbI_3$ nucleates separately, their corresponding PL and absorption peaks should appear.[38,39]

As observed above, the increase in Sn portion significantly enhances the light absorption of the alloyed $CsSn_{1-x}Pb_xI_3$ QDs, however, this also results in QDs with extremely low PL quantum yields of 0.3%~3.0% (x = 0.4~0.8). In comparison with the typical high quantum yields of ~90% obtained in the pure $CsPbI_3$ QDs, the observed severe PL degradation in our alloyed QDs is believed to result from the increase in intrinsic defects that are associated with Sn vacancies (V_{Sn}), which have very low defect formation energies of ~250 meV.[26] These vacancies can thus form easily and produce a high p-type conductivity as well as deep-level defects that act as nonradiative recombination centers and hence reducing the efficiency of radiation.[22,26,28,40] To understand such a decrease in PL quantum efficiency, we therefore carried out time-resolved PL decay measurements. PL decay dynamics shown in Figure 1d reveal two different PL decay processes in $CsSn_{1-x}Pb_xI_3$ QDs, which means the presence of two different exciton relaxation pathways in the QDs. The slow component has time constants of 13~20 ns with weight fraction from 2% to 7%, while the fast radiative lifetimes were calculated in the range of 0.1~1.2 ns with weight fraction from 93% to 98% (the details of the fluorescence lifetimes for the alloyed QDs with different stoichiometries are summarized in Table S2, Supporting

Information). Average lifetime of the alloyed QDs can be estimated to be 7.7~11.6 ns by use of the expression of intensity-weighted average lifetime, $\tau_{ave} = (a_1\tau_1^2 + a_2\tau_2^2)/(a_1\tau_1 + a_2\tau_2)$,[41] which was found to dramatically decrease with increasing Sn content. Compared with the long radiative lifetimes typically obtained in the pure $CsPbI_3$ QDs (~54 ns), the extremely short-lived, yet is also dominating radiative relaxation thus confirms the presence of large density of quenching defects in these Sn-contained perovskites, consistent with the observation of their low PL quantum yields.

In order to gain more insight about the photophysical properties of the resulting alloyed QDs, we further investigate the Urbach energies in these QDs by plotting their absorption coefficient as a function of photon energy (Figure 1e). In semiconductors and insulators, the fundamental absorption edge below the energy band gap increases exponentially, and the absorption edge is known as the Urbach tail.[42] Fitting the exponential part of the Urbach tail with the following Urbach's rule (eq. (1)) allows us to extract the Urbach energy (E_U), which represents the absorption tail states of these materials and is closely related to the degree of electronic disorder within the crystals.[42]

$$\alpha(E) = \alpha_0 \exp\left[\sigma(T)\frac{E - E_0}{k_B T}\right] \quad (1)$$

where $\alpha(E)$ is the absorption coefficient as a function of photon energy E, E_0 and α_0 are the characteristic parameters of the material, $\sigma(T)$ is the steepness factor, k_B is the Boltzmann constant, and T is the absolute temperature. The Urbach energy is defined as $E_U = k_B T/\sigma(T)$. A large E_U value is a strong indicator that the samples suffer from a cumulative effect of impurities, inherent structural disorders, and electron-phonon interaction in the absorption processes.[43-45] Figure 1e shows the typical room-temperature logarithmic absorption coefficient of the $CsSn_{1-x}Pb_xI_3$ QDs as a function of photon energy. Urbach energies derived by fitting eq. (1) to each exponential tail shown in Figure 1e are summarized in Figure 1f. It is seen that E_U values increase remarkably from 20 to 44 meV with Sn mole proportion increasing

from 0 to 1. This result indicates that increasing Sn concentration induces a higher level of electronic disorder and/or defect density in the QDs, which is in good consistent with the dependences of the PL QY and radiative lifetimes of the $CsSn_{1-x}Pb_xI_3$ QDs on the Sn mole proportion.

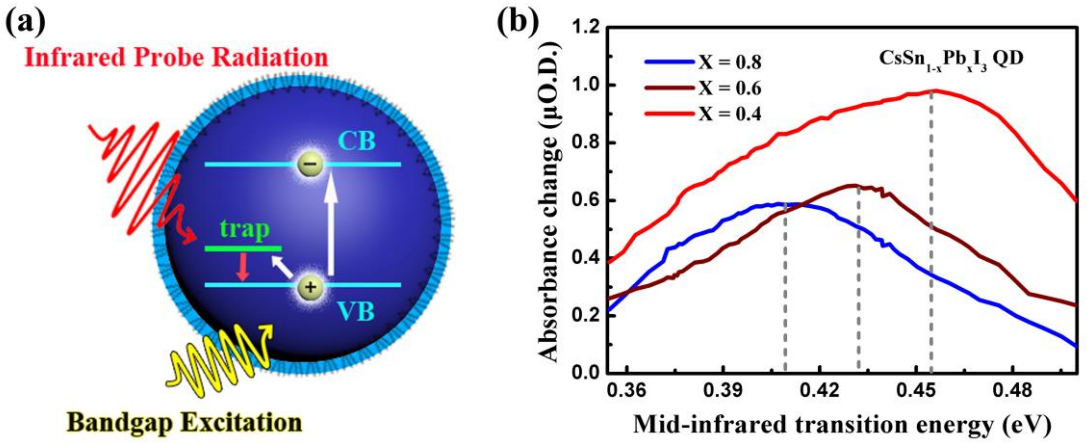

Figure 2. (a) Schematic diagram illustrating the trap-to-band transitions observed in TRIR transient absorption spectra. (b) TRIR spectra of the $CsSn_{1-x}Pb_xI_3$ QD films measured at the maximum of the absorption change after bandgap excitation.

We then carried out time-resolved infrared (TRIR) spectroscopy experiment to qualitatively describe the quenching defects in these resulting $CsSn_{1-x}Pb_xI_3$ QDs. TRIR measurement allows the direct examination of the charge traps in QDs through excitation of carriers from trap states into band states of the QDs.[46,47] The schematic in Figure 2a depicts pictorially the photophysical sequence that gives rise to the transient infrared absorption process for the case of trapped holes from the trapping states (p-type) to the valence band. TRIR spectra presented in Figure 2b were recorded for $CsSn_{1-x}Pb_xI_3$ QD films with different Sn mole proportions at their maximum absorption change after bandgap excitation, where a broad characteristic feature can be observed for each sample, which results from transitions of holes from localized states (band-tail or trap states) to delocalized states of the QDs. The peak position and amplitude of the spectra reflect the depth and number of the trapped carriers, respectively.[46,47] Comparison of the TRIR spectra shown in Figure 2b reveals

that holes (p-type) are trapped in energetically deeper trap states in Sn-rich QDs (0.4~0.5 eV above the valence band). Meanwhile, the amplitudes of the trap-to-band transitions obviously increase with the Sn content, indicating a higher trap density in those Sn-rich QDs. As described above, the possible reason for these trap states is the presence of large density of Sn vacancies in Sn perovskites. The above results also agree very well with the previous Urbach energy analysis and support the observation of the low quantum yields in those Sn-rich QDs.

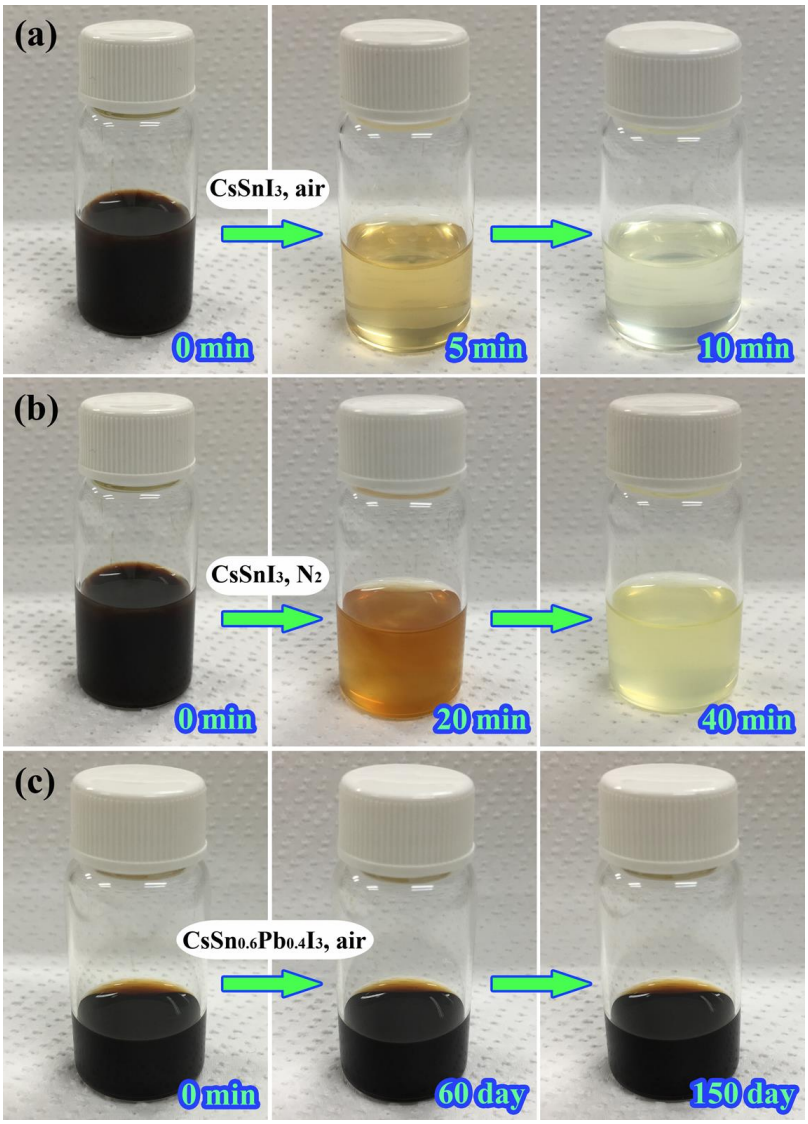

Figure 3. Photographs taken at different period of time for solutions of the as-synthesized $CsSnI_3$ QDs (a) stored in ambient air and (b) stored under nitrogen atmosphere. (c) $CsSn_{0.6}Pb_{0.4}I_3$ QDs after twice MeOAc washing and stored in ambient air. All samples including $CsSnI_3$ and the purified $CsSn_{0.6}Pb_{0.4}I_3$ QDs were dispersed

in hexane.

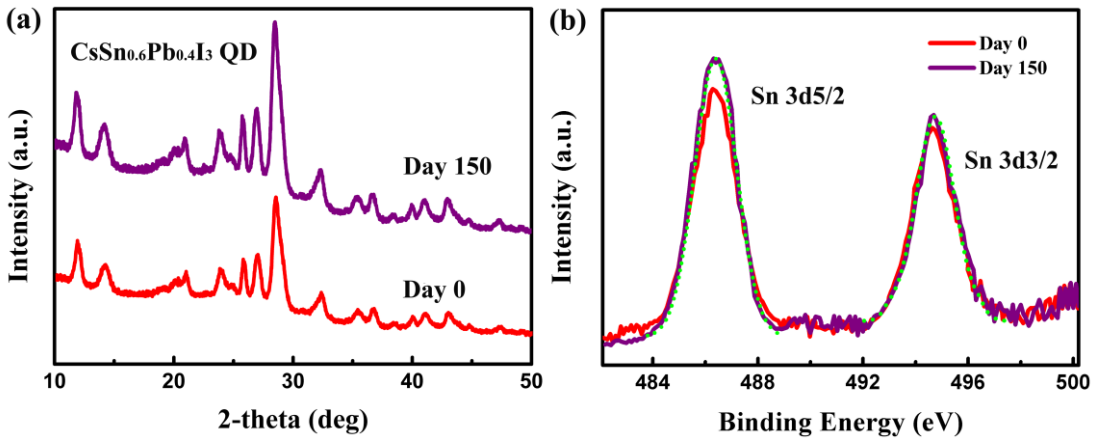

Figure 4. (a) XRD patterns and (b) XPS spectra of Sn 3d recorded for the fresh $CsSn_{0.6}Pb_{0.4}I_3$ QD sample (purified twice) and those after storage in solution for 150 days. Green short dot lines in **(b)** represent fitting results of the peak signal.

Fortunately, with regarding to the disadvantage of the decreased PL quantum yields caused by the introduction of quenching defects in these Sn-contained perovskites, previous studies have demonstrated that chemical doping with tin halides (*e.g.*, SnF_2, $SnCl_2$, and $SnBr_2$) could effectively suppress the formation of Sn vacancies and thus reduce the trapping defects.[18,22,25,27,28] As for the case of our alloyed Sn/Pb perovskite QDs, we can also expect such doping approach to reduce their trapping defects. However, as pointed out in *Introduction*, stability problem of these tin or lead perovskites still remains unsolved and has now become the main barrier for their successful use in either solar cells or LEDs, *etc*. Therefore, next, we shall mainly focus on investigating the alloying effect on both phase and structure stability of the resulting QDs. First, colloidal stability of the alloyed QDs was compared to that of the pure $CsSnI_3$ QDs. Here, $CsSn_{0.6}Pb_{0.4}I_3$ is chosen because among the alloyed QDs examined, $CsSn_{0.6}Pb_{0.4}I_3$ QD is of most interest as it contains less content of Pb but possesses the most wide range of light absorption. Figure 3 shows photographs of solutions of $CsSnI_3$ and $CsSn_{0.6}Pb_{0.4}I_3$ QDs taken at different period of time. It is observed that the reference as-synthesized $CsSnI_3$ QD solution changes color from

black to yellow within a very short period of time whether it is exposed to ambient air or stored under nitrogen atmosphere, leaving a yellow precipitate and clear supernatant. This observation also confirms a very fast phase transition and particle aggregation occur in the as-synthesized B-γ $CsSnI_3$ QDs. In contrast, the twice-washed $CsSn_{0.6}Pb_{0.4}I_3$ QDs dispersed in hexane do not show any apparent change in color over a span of 5-month observation period, suggesting a much superior stability to that of the pure $CsSnI_3$ QDs. UV-vis absorption spectra recorded for both kinds of QDs shown in Figure S6 further confirm this color observation. Direct evidence for the improved phase stability of the alloyed QDs was presented in Figure 4a, which shows nearly identical XRD patterns between the fresh $CsSn_{0.6}Pb_{0.4}I_3$ QDs and those after storage for 5 months. Figure 4b gives high-resolution XPS spectra taken of the Sn region for the fresh $CsSn_{0.6}Pb_{0.4}I_3$ QDs and those aged. The two peaks observed in the measured spectra at 486.2 and 494.5 eV are associated with divalent Sn 3d5/2 and 3d3/2, respectively,[39,48-50] which are barely changed during 5-month observation period. In addition, no SnO_2 (~486.9 eV) or zero-valent Sn signal (~484.9 eV) could be detected from fitted curves of the Sn XPS after 150 days storage (Figure 4b), suggesting that the oxidation or reduction of Sn^{2+} was successfully inhibited in the alloyed QD solution.

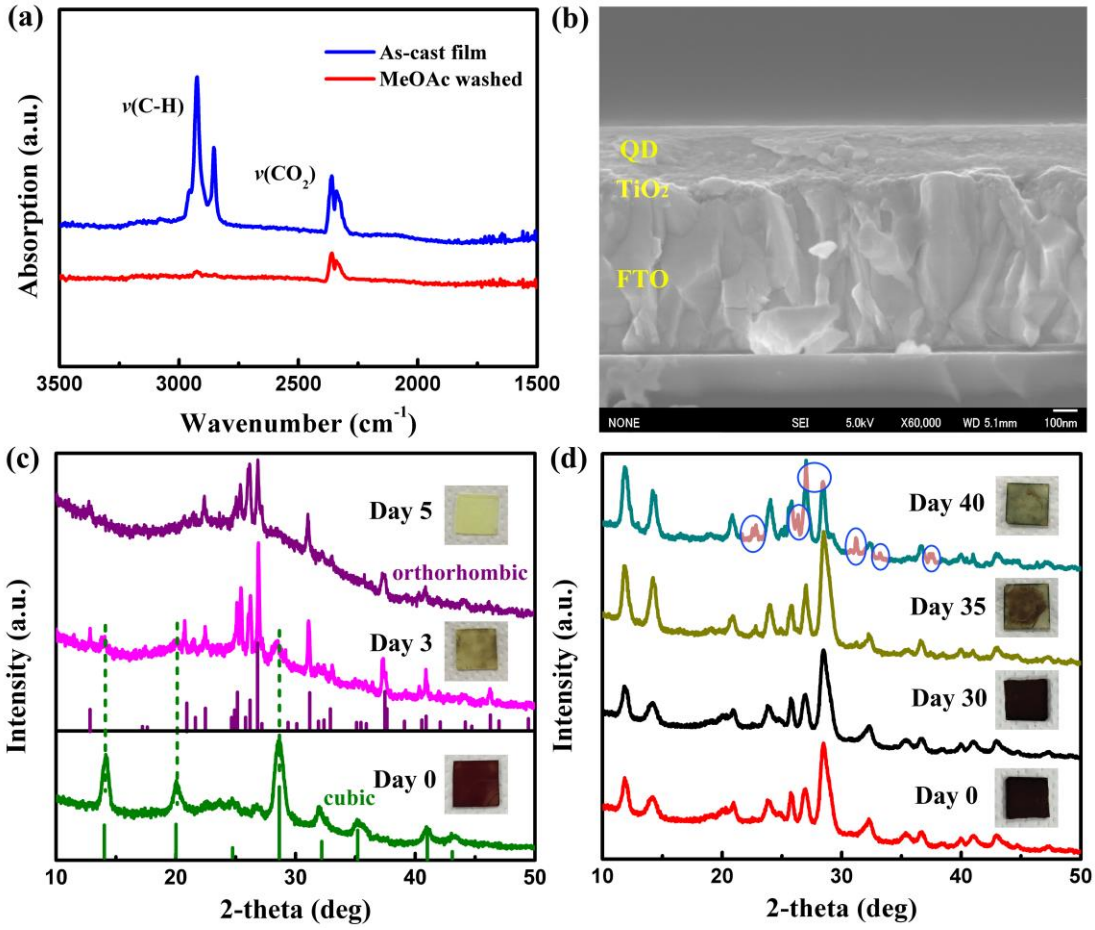

Figure 5. (a) FT-IR spectra of a $CsSn_{0.6}Pb_{0.4}I_3$ QD film as cast (black) and after washing with MeOAc (red). (b) Cross-section scanning electron microscope (SEM) image of the $CsSn_{0.6}Pb_{0.4}I_3$ QD thin films. (c) XRD patterns recorded at different period of time for the $CsPbI_3$ and (d) $CsSn_{0.6}Pb_{0.4}I_3$ QD thin films deposited on a glass substrate. All samples were stored under ambient conditions with relative humidity of 30~40%.

Air-stability of the alloyed QDs was further evaluated by comparing their XRD spectra with that of the pure $CsPbI_3$ QDs in the form of solid thin films and exposing them directly to air (note that the MeOAc-washed $CsPbI_3$ QDs can be phase-stable for ~3 months in colloidal solution). QD solid films studied here were prepared according to the method proposed by Luther *et al*. with little modification.[1] First, in a N_2-filled glovebox, 100 μL of QD solution (50 mg/mL in octane) was deposited on a glass or a FTO/dense TiO_2 substrate, and spin-cast at 2000 rpm (FTO/TiO_2 substrate was

prepared as described in Supporting Information). Then, those long-chain unbound ligands and other organic impurities in the as-cast films were removed by flooding the surface with MeOAc for 3 s before spin-coating dry at 2500 rpm for 30 s. The above deposition-washing process was repeated 5 times so as to produce dense QD films with a considerable thickness. Figure 5a shows the FT-IR spectra of a $CsSn_{0.6}Pb_{0.4}I_3$ QD film as cast and after washing with MeOAc, which evidence the removal of those residual organics in the MeOAc-washed sample, given that the strong C-H bending vibration peaks at 2853 and 2923 cm^{-1} assignable to the hydrocarbon chains from organic species are significantly reduced. Figure 5b shows cross-section SEM image of a prepared QD thin film sample deposited on the FTO/TiO_2 substrate, where a 200-nm-thick compact QD layer can be clearly identified. For stability test, all samples were taken out from glovebox and exposed directly to ambient air with relative humidity of 30~40% (25 °C). Figure 5c shows that the $CsPbI_3$ QD thin films gradually degrade into the inactive yellow phase, where peaks characteristic of the orthorhombic phase appeared and became dominant within 3 days of exposure to air. This observation is consistent with Luther *et al.*'s report, in which a notable decrease in photovoltaic performance was recorded for $CsPbI_3$ QD thin film solar cells after storage for 2 days in humid conditions.[1] In contrast, $CsSn_{0.6}Pb_{0.4}I_3$ QD thin films show a surprisingly high stability as their XRD patterns remain unchanged even after 1-month storage in air (Figure 5d). But after 1-month storage, like most of the other perovskites, $CsSn_{0.6}Pb_{0.4}I_3$ QDs slowly degrade into the yellow phase as evidenced by their noticeable change in film color and XRD patterns (marked with circles in the figure), which is likely to result from a moisture-driven degradation process.

We consider the improved phase/air stability of the alloyed Sn perovskites does not come from the protective effect of those hydrophobic organic ligands because $CsSnI_3$ QD alone synthesized in our study, even capped with thick protecting organic ligands, is also extremely unstable as they rapidly transform into the yellow phase within minutes in air. However, in contrast, even most of the organic ligands are stripped from surface of our alloyed $CsPb_{1-x}Sn_xI_3$ QDs, they can be still phase-stable and valence-stable in air for one month (organic ligands are removed from QD surface

through 3~4 times of repeated precipitation/redissolution process using MeOAc, after such treatment, we can see the resulting QD precipitate can be no longer redispersed in hexane because of the loss of QD surface ligands). It is worth mentioning that the superior stability observed in these alloyed QDs even in the absence of protecting ligands is in line with a very recent experiment result reported by Liang *et al.*, where bulk thin film $CsPb_{0.9}Sn_{0.1}IBr_2$ perovskites prepared under ambient conditions show excellent long term stability and highly-improved endurance against heat and moisture.[51] One possible reason for the improved oxidation stability of our alloyed Sn perovskites could be associated with the new formed stable crystal structure when alloying with $CsPbI_3$ (revealed by XRD measurement), which results in a higher binding energy of ~486.2 eV for Sn^{2+} (Sn 3d5/2, shown in Figure 4b) than that in the pure $CsSnI_3$ (~485.2 eV),[52,53] and thus a higher resistance to oxidation.

The improved phase stability observed in our alloyed QDs also agrees very well with that in Luther *et al.*'s report, where perovskites in the form of QDs were shown to possess a much higher phase stability than that in bulks. They attribute the higher stability of the QDs to their confined size and large contribution of the surface energy.[1] Moreover, we note that the air-stability of the alloyed QDs is closely related to the content of Sn. It is normally thought that increasing Sn concentration in the alloyed QDs would lead to an inferior stability since $CsSnI_3$ is less stable compared with $CsPbI_3$.[21,24,36] However, on the contrary, within a certain range, *i.e.*, for Sn mole proportion ranging from 0.2-0.6, we found that increasing Sn content would yield alloyed QDs with a better resistance to air exposure as well as better colloidal stability in solution. We rule out the possibility that the improved air stability comes from the possible formation of layered low-dimensional structures which typically demonstrate a better stability than their three-dimensional (3D) counterparts due to the separation of perovskite sheets from moisture and oxygen *via* encapsulation of the organic ligands,[54-57] because XRD spectra scanned at smaller angles show that our alloyed QDs do not have diffraction signal peaks below 10°, which is actually a typical feature of those 2D perovskites.[54-57] Besides, previous studies on 2D Sn perovskites also show that although these low-dimensional Sn perovskites exhibit enhanced

stability when compared to their 3D counterparts, they could still only survive less than 1 hour in ambient air, far shorter than here observed in our case.[55,58,59] In fact, we notice that our experimental results of the increased air-stability in these alloyed Sn/Pb perovskites with increasing Sn concentration are in good agreement with a recent computation study, where a similar stability trend is demonstrated in those of the Sn-dominated conditions. The authors attribute this behavior to the difference in geometric tolerance factor because of the different ionic radiuses (R) between Sn^{2+} and Pb^{2+}.[60] Geometric tolerance factor (T) is defined as follows:

$$T = \frac{R_{cs} + R_I}{\sqrt{2}\left(R_{Pb/Sn} + R_I\right)} \qquad (2)$$

Since Sn^{2+} has a smaller ionic radius (R_{Sn} = 0.93 Å) than that of Pb^{2+} (R_{Pb} = 1.19 Å), the more Sn that is introduced in the alloyed system, the higher the tolerance factor will be and thus of the stability of the perovskite structure (the calculated T is 0.88 for the pure $CsSnI_3$, whereas it is 0.81 for $CsPbI_3$). On the other hand, the Sn-I bond length is shorter than that of Pb-I, which also favors the formation of stable perovskite lattice.[60] The above considerations are also in agreement with a recent reported observation of Mn alloyed $CsPbI_3$ perovskites that demonstrate enhanced stability like ours. They attribute the improved stability to the small decrease in the lattice parameters that slightly increases the Goldsmith tolerance factor, combined with an increase in the cohesive energy.[61] Consistently, Eperon *et al*. foretold and implied that alloying B-site in Pb perovskites (ABX_3) with smaller divalent metals, such as Mn^{2+}, Co^{2+}, and Hg^{2+}, *etc*. would have significant impact on the stability of the materials.[62] However, although we recognize the positive role of introducing Sn on enhancing structure stability of the perovskites, we believe that the improved ambient stability of these alloyed QDs is a coupled effect of Sn and Pb because even though the mere Sn composition has a larger tolerance factor, it is still not phase-stable.

The improved phase and colloidal stability of the alloyed QDs being attributed to the coupled effect of Sn and Pb may be also understood as follows: First, it is known that the stable and unstable $CsPbI_3$ perovskites crystallize into two different crystal structures, one is orthorhombic phase, which is thermodynamically stable (space

group *Pnma* with lattice constants of *a* = 4.797 Å, *b* = 10.460 Å, *c* = 17.780 Å), and the other is active but unstable cubic phase (space group *Pm-3m* with lattice constant a = b = c = 6.2 Å).[63] While, interestingly, for both stable and unstable $CsSnI_3$, they all adopt orthorhombic structure, only with different lattice constants of the unit cell. Specifically, the stable orthorhombic phase $CsSnI_3$ crystallizes in space group *Pnma* with lattice constants of *a* = 4.763 Å, *b* = 10.350 Å, *c* = 17.684 Å, while the active but unstable one crystallizes in space group *Pnma* with lattice constants of *a* = 8.689 Å, *b* = 12.378 Å, *c* = 8.638 Å.[21] Therefore, through colloidal synthesis and combining the active cubic $CsPbI_3$ with the active orthorhombic $CsSnI_3$, it is entirely possible that the resulting alloyed QDs crystallize into active orthorhombic phase, and meanwhile maintain stable structure because both parent $CsSnI_3$ and $CsPbI_3$ can be stable in orthorhombic phase.

Thermal stability of the resulting $CsSn_{0.6}Pb_{0.4}I_3$ QD composition was further evaluated using thermogravimetric analysis (TGA) measured under nitrogen flow from room temperature to 500 °C as shown in Figure S7. The TGA spectrum shows that the alloyed perovskite QD crystal can be thermally stable up to 320 °C, comparable to that of the previously reported bulk $CsPbI_3$ and higher than that of those organic-inorganic hybrid perovskites.[64-66] It is also worth noting that the main diffraction peak positions in XRD spectra of the alloyed QDs remain unchanged even they are heated up to 250 °C in nitrogen, while as observed in previous report, once the $CsPbI_3$ QD sample temperature reached 213 °C, its active cubic phase would promptly transform to the yellow orthorhombic structure,[1] indicating a superior thermal stability of the alloyed QDs.

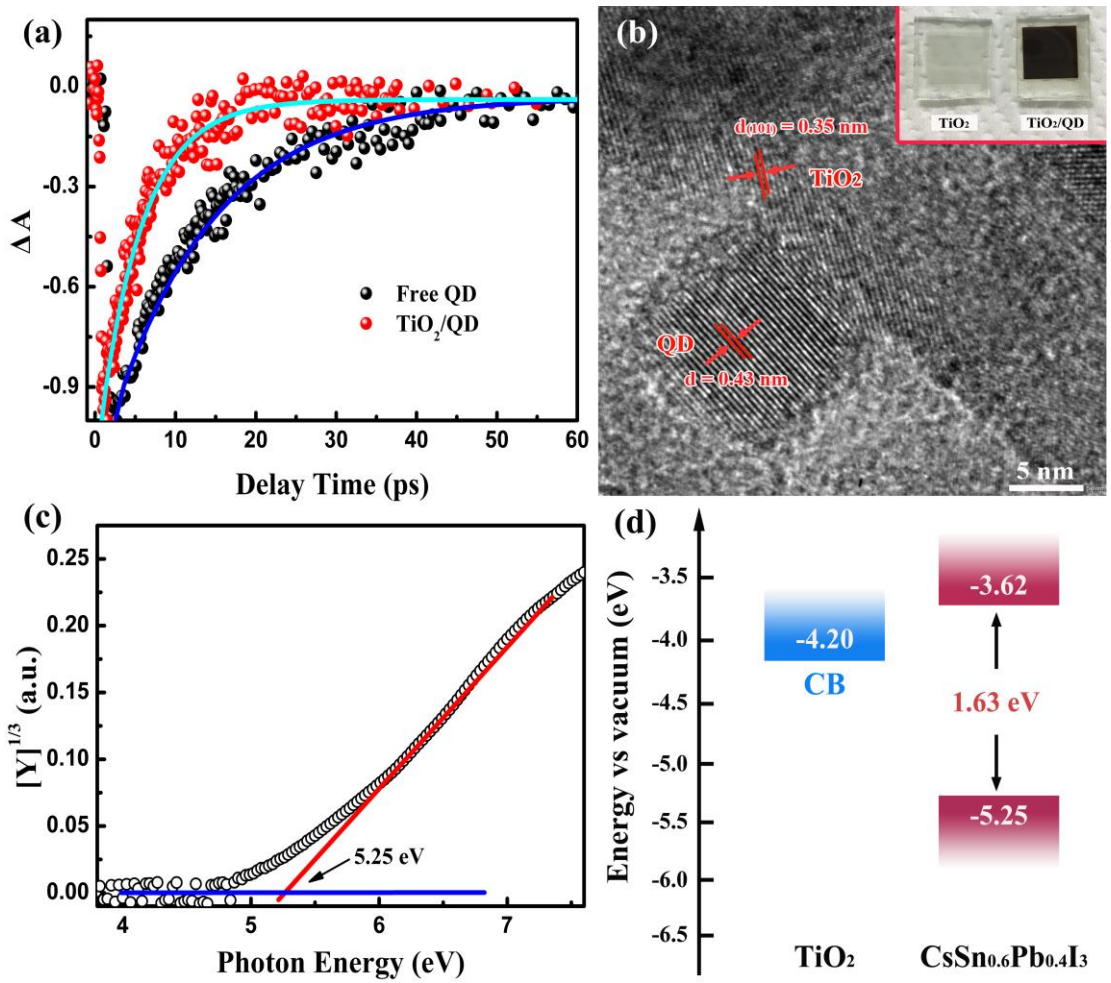

Figure 6. (a) TA responses of the free $CsSn_{0.6}Pb_{0.4}I_3$ QDs and TiO_2-QD composite measured with a pump light wavelength of 470 nm and probe light wavelengths of 760 nm. Pump light intensity: 12.9 $\mu J/cm^2$. (b) HRTEM image of the TiO_2-QD composite. The measured interplanar spacing of 0.35 nm and 0.43 nm respectively confirm the presence of $CsSn_{0.6}Pb_{0.4}I_3$ QDs on TiO_2 surface. The inset shows photographs of the TiO_2 film before (left) and after (right) incorporation of the QDs. (c) PYS spectrum of the 14 nm-diameter $CsSn_{0.6}Pb_{0.4}I_3$ QDs. (d) Schematic energy level diagrams of the TiO_2 and $CsSn_{0.6}Pb_{0.4}I_3$ QDs.

The successful synthesis of the stable $CsSn_{0.6}Pb_{0.4}I_3$ QDs now allows us to further explore the fundamental physics behind these interesting Sn-contained perovskites and would be expected to greatly expand their possibilities for use in various applications. For example, Hall measurements reveal that the prepared $CsSn_{0.6}Pb_{0.4}I_3$ QD thin films exhibit *p*-type conducting behavior with a carrier mobility of 40.12

$cm^2/V{\cdot}s$, close to the values measured for bulk $CH_3NH_3PbX_3$ thin films,[67] thus being promising for use in a wide range of optoelectronic applications. To investigate their potential use as light-absorbing material in solar cells, we next carried out ultrafast TA spectroscopy studies of the dynamics of photogenerated excitons within $CsSn_{0.6}Pb_{0.4}I_3$ QDs and the injection of these photoexcited electrons from QDs into TiO_2 nanocrystallines. $CsSn_{0.6}Pb_{0.4}I_3$ QDs with ~14 nm diameter dispersed in hexane were prepared through colloidal synthesis at 160 °C and purified twice with MeOAc before measurement. Figure S8 records the TA spectra of the free $CsSn_{0.6}Pb_{0.4}I_3$ QDs in solution measured at a pump light intensity of 25.8 $\mu J/cm^2$, in which bleach signals with peak at 760 nm can be clearly observed, corresponding to the optical absorbance change (ΔA) between the LUMO and HOMO in the $CsSn_{0.6}Pb_{0.4}I_3$ QDs. In this case, it is known that the ΔA is proportional to the exciton density *n* at the lowest excited states in the QDs.[68-70] In consideration of the possible one-body, two-body, and three-body recombination processes within a single QD, TA decay curves can be represented by the following equation (3):[71]

$$dn/dt = An + Bn^2 + Cn^3 \quad (3)$$

where *An* represents single-body behavior (*i.e.*, electron and/or hole trapping), Bn^2 represents two-body radiative recombination (*i.e.*, PL emission), and Cn^3 represents three-body nonradiative Auger recombination process. Figure S9 shows the normalized TA decays of the $CsSn_{0.6}Pb_{0.4}I_3$ QDs under different pump excitation intensities with probing wavelengths of 760 nm. It is found that, regardless of the intensity of pump light used, the waveforms of the TA responses overlapped with each other very well when they are normalized at the peak intensity. This phenomenon indicates the absence of three-body Auger recombination process in our $CsSn_{0.6}Pb_{0.4}I_3$ QDs, and only one-body and two-body recombination processes can be observed here.[68-70] The dotted black line in Figure 6a shows the exciton bleach signal of the free $CsSn_{0.6}Pb_{0.4}I_3$ QDs measured with a pump light intensity of 12.9 $\mu J/cm^2$. The kinetic

traces shown by the blue solid line can be well fitted using the following bi-exponential function (4), which gives two exponential decay constants, τ_1 of 12.8 ps ($A_1/(A_1+A_2+y_0)$ = 99.6%), τ_2 of 80.7 ps ($A_2/(A_1+A_2+y_0)$ = 0.39%), and a constant component y_0 with $y_0/(A_1+A_2+y_0)$ = 0.01%.

$$Y(t) = A_1 \exp(\frac{-t}{\tau_1}) + A_2 \exp(\frac{-t}{\tau_2}) + y_0 \quad (4)$$

As discussed above, this result means that about 99.6% of the photoexcited electrons recombine through one-body recombination process and the rest ~0.4% recombine through two-body recombination pathway (*i.e.*, PL radiative recombination). In particular, the measured TA exponential decay lifetime of 80.7 ps matches well with the previous PL decay measurements, in which a dominant exciton decay component with lifetime of ~0.1 ns can be resolved from PL decay spectra of the $CsSn_{0.6}Pb_{0.4}I_3$ QDs. Overall, the above TA results confirm that the decay dynamics of the resulting $CsSn_{0.6}Pb_{0.4}I_3$ QDs is dominated by the intrinsic defects in the QDs, which also explains their low measured PL quantum yields of ~0.3%. As discussed early, these intrinsic defects are mainly associated with Sn vacancies in Sn perovskites, which form deep-level trap state 0.4~0.5 eV above the valence band.

To probe charge transfer from the photoexcited $CsSn_{0.6}Pb_{0.4}I_3$ QDs into nanocrystalline TiO_2, TA measurements were further performed on QD-TiO_2 composite. QD-TiO_2 composite sample was prepared according to the prototype photoanode configuration in a QD-sensitized solar cell, where TiO_2 nanoparticles are typically adsorbed with a monolayer of QD sensitizer, photoexcited electrons in the QDs can be thus injected into the TiO_2 matrix and photocurrent is generated.[72-76] Such monolayer adsorption scheme would thus rule out the possibility of charge transfer between neighbour QDs. Here, $CsSn_{0.6}Pb_{0.4}I_3$ QD monolayers were self-assembled onto TiO_2 surface by directly immersing the mesoporous TiO_2 films into a prepared QD solution (see Supporting Information for more details). Astonishingly, saturated adsorption of the alloyed QDs onto TiO_2 films (as shown in the inset of Figure 6b) can

be completed within 2 mins, much faster than those of the traditional QDs like CdSe and InP, which typically require several hours or days.[77-79] The adsorption of the alloyed QDs onto TiO_2 surface is clearly evidenced by a typical HRTEM image shown in Figure 6b, where a single $CsSn_{0.6}Pb_{0.4}I_3$ QD is adsorbed on the TiO_2 nanoparticle and clear lattice fringes of both the QD and the TiO_2 can be well resolved. Interestingly, from HRTEM observation, we also noticed that there is an epitaxial interface between the TiO_2 and the QDs, suggesting the direct contact and the loss of surface ligands at the interface of QD/TiO_2. Such ligand detachment from surface of the QDs is also implied in Guijarro *et al*.'s study, where part of the surface ligand on CdSe QDs was removed when QDs are directly contacted with TiO_2.[80] In fact, as demonstrated by Pernik *et al*., ligand removal from QD surface can greatly accelerate their adsorption to TiO_2,[77] which also explains the fast QD adsorption observed in our case. The dotted red line in Figure 6a shows TA trace of the $CsSn_{0.6}Pb_{0.4}I_3$ QDs adsorbed on the TiO_2 which works as electron acceptor. Again, the QD-TiO_2 sample was excited and probed with light wavelengths of 470 nm and 760 nm, respectively, same as used in the case of free QDs without TiO_2. The TA response of the QD-TiO_2 composite can be well fitted using the following single-exponential equation (5), which gives a time constant τ_{TiO2} of 5.2 ± 0.2 ps with $A_0/(A_0+y_0)$ = 99%.

$$Y(t) = A_0 \exp(\frac{-t}{\tau}) + y_0 \quad (5)$$

Then the electron transfer rate k_{et} ($k_{et} = 1/\tau_{et}$, where τ_{et} is the electron transfer time from the QDs to TiO_2) can be calculated to be 1.12×10^{11} s^{-1} by using $k_{et} = 1/\tau_{TiO2} - 1/\tau_1$. The observed electron transfer rate at a sensitizing $CsSn_{0.6}Pb_{0.4}I_3$ QD-TiO_2 interface is comparable to that of the traditional PbS QD/TiO_2 sensitizing system, which typically exhibits fast electron transfer rate of ~1×10^{11} s^{-1} (*i.e.*, electron transfer time of ~10 ps).[81] Notably, such an injection rate in our $CsSn_{0.6}Pb_{0.4}I_3$ QDs/TiO_2 is faster than that in $CsPbBr_3$ QD-benzoquinone complex system, which shows electron transfer rate of ~1.5×10^{10} s^{-1} (*i.e.*, electron transfer time of ~65 ps).[82]

The efficient interfacial electron injection from $CsSn_{0.6}Pb_{0.4}I_3$ QDs to TiO_2 can be rationalized by the observation of their energy level alignments, which are determined by photoelectron yield spectroscopy (PYS) measurement. Figure 6c shows PYS spectrum of the 14 nm-diameter $CsSn_{0.6}Pb_{0.4}I_3$ QDs, from which valence band energy (E_{VB}) of the QDs is estimated to be -5.25 eV below vacuum level. Combining with the previously recorded optical band gap of 1.63 eV in Figure S8, the conduction band energy (E_{CB}) of the $CsSn_{0.6}Pb_{0.4}I_3$ QDs can be thus determined to be -3.62 eV, which is much higher than that of TiO_2 (-4.20 eV). The schematic band alignment is sketched in Figure 6d, where the band positions are well aligned for charge separation. The above observations thus confirm that the synthesized alloyed QDs hold great promise for use in solar cells and potentially enable a high photocurrent generation for the solar cells.

In order to demonstrate their practical use in photovoltaics, we have tested solid-state heterojunction thin film solar cells fabricated with our $CsSn_{0.6}Pb_{0.4}I_3$ QDs (FTO/compact-TiO_2/mesoporous-TiO_2/QD/Spiro-OMeTAD/Au, and the details of the solar cell fabrication can be found in Supporting Information), where the QD layer is about 400 nm. The prepared QD heterojunction solar cells can be stable for month in air but exhibit extremely low power conversion efficiency of 0.1% with J_{sc} of 0.26 mA/cm^2, V_{oc} of 0.90 V, and FF of 0.42. The low efficiency mostly results from the low J_{sc} and the low J_{sc} is very likely because of the residual bound ligands on QD surface in the active layer of the solar cells, which retard charge transport through the thin films (because unlike the individual QDs whose surface ligands can be almost completely removed through multi-times precipitation/redissolution process using MeOAc, the ~400 nm QD layers prepared here with the present method for solar cell devices may still contain a certain amount of organics, as evidenced by its FT-IR spectrum which shows non-negligible ν(C-H) signal in Figure 5a, red line).

With regarding to the potential problem of the insufficient charge transport caused by these very insulating long-chain ligands, previous studies have demonstrated that complete ligand exchange with shorter ligands or inorganics would greatly improve the charge transfer between QDs and hence increase the photocurrent of the solar

cells.[46,47] However, unfortunately, these reported ligand exchanging methods generally require the use of those strong polar solvents like DMF and water, which will inevitably destroy our prepared perovskite QDs. Therefore, suitable ligand exchange or washing method is required to further improve the efficiency of the QD thin film solar cells.

Quantum dot-sensitized solar cell (QDSC) is another important photovoltaic technology for solar energy conversion, where QD monolayer (or 2~3 layers) deposited on a wide band gap nanostructured semiconductor (*e.g.*, TiO_2, ZnO, SnO_2) acts as light-absorbing material, in the same configuration as in dye-sensitized solar cells (DSCs).[83-85] In QDSCs, since the main charge separation and transfer take place at the interface of QD monolayer/TiO_2, the single thin layer of organic ligands will impose less impact on the charge collection of the nanostructured semiconductors. Besides, as observed in our case (Figure 6b), the adsorption of the colloidal QDs on TiO_2 surface is usually accompanied by the loss of part of the surface ligands at the interface of QD/TiO_2, interfacial charge transfer will be thus greatly promoted. In fact, as studied above, through TA measurement, we have shown that photoexcited electrons in the $CsSn_{0.6}Pb_{0.4}I_3$ QDs can be injected into TiO_2 at a fast rate of 1.12×10^{11} s^{-1}. We therefore fabricated prototype QDSCs with $CsSn_{0.6}Pb_{0.4}I_3$ QDs as the sensitizer and liquid-state iodide electrolyte (I^-/I_3^-) was employed, which deliver enhanced J_{sc} of 10.13 mA/cm^2 (details of the fabrication can be found in Supporting Information). But the overall efficiency of 2.9% (V_{oc} = 0.63 V and FF = 0.46) is still far from what we had expected, which is mainly caused by the mismatch between QDs and the used liquid-state iodide electrolyte, which even induce a severe degradation of the QD sensitizers. Considering that no attempt was made to optimize the performance (*e.g.*, Sn/Pb ratio, electrolyte, and TiO_2 film thickness, *etc.*), the results are encouraging, and we notice that the efficiency obtained at this stage is quite close to that of the first solar cell demonstration of the nanocrystalline $CH_3NH_3PbI_3$, which employed the same configuration and the same I^-/I_3^- electrolyte as ours, and exhibited efficiency of 3.8%.[86] We expect that significant improvement can be made through the use of alternative electrolytes, such as quasi-solid

electrolytes as used in DSCs,[87,88] or solid-state hole transport materials like P3HT and PCPDTBT (*i.e.*, to fabricate all-solid-state QDSCs),[89-91] and these are under way.

Conclusions

In conclusion, we have presented a facile reproducible synthetic route to the alloyed $CsSn_{1-x}Pb_xI_3$ QDs, which exhibit far superior stability than both of its parent $CsSnI_3$ and $CsPbI_3$ QDs. These alloyed perovskite QDs can be readily extracted from the as-synthesized crude solution and phase-stable for months whether stored in solution or directly exposed to ambient air, being promising for use in various applications. TA spectroscopy studies reveal that the photoexcited electrons in the alloyed QDs can transfer into the nanocrystalline TiO_2 at a fast rate of 1.12×10^{11} s^{-1}, which enables a high photocurrent generation in solar cells. In addition, in light of these findings, we foresee the alloying strategy presented here may be extended to other perovskite compositions and open up new possibilities for enhancing the stability of these amazing but susceptible materials.

Associated content

Supporting Information

Experimental details, additional NMR, TEM images, UV-vis absorption spectra, XPS spectra, XRD, PL lifetimes, TGA, TA responses of alloyed QDs, and PYS spectrum. This material is available free of charge *via* the Internet at http://pubs.acs.org.

Author Information

Corresponding Author

shen@pc.uec.ac.jp

hayase@life.kyutech.ac.jp

Notes

The authors declare no competing financial interest.

Acknowledgements

This research was supported by the Japan Science and Technology Agency (JST) CREST program, JST PRESTO program, the MEXT KAKENHI Grant (Grant Number 26286013, 17H02736) and the UEC postdoctoral program.

References

(1) Swarnkar, A.; Marshall, A. R.; Sanehira, E. M.; Chernomordik, B. D.; Moore, D. T.; Christians, J. A.; Chakrabarti, T.; Luther, J. M. *Science* **2016**, *354*, 92.

(2) Song, J. Z.; Li, J. H.; Li, X. M.; Xu, L. M.; Dong, Y. H.; Zeng, H. B. *Adv. Mater.* **2015**, *27*, 7162.

(3) Ramasamy, P.; Lim, D. H.; Kim, B.; Lee, S. H.; Lee, M. S.; Lee, J. S. *Chem. Commun.* **2016**, *52*, 2067.

(4) Sutherland, B. R.; Sargent, E. H. *Nat. Photonics* **2016**, *10*, 295.

(5) Kamat, P. V. *ACS Energy Lett.* **2017**, *2*, 1128.

(6) Cortecchia, D.; Dewi, H. A.; Yin, J.; Bruno, A.; Chen, S.; Baikie, T.; Boix, P. P.; Grätzel, M.; Mhaisalkar, S.; Soci, C. *Inorg. Chem.* **2016**, *55*, 1044.

(7) Saparov, B.; Hong, F.; Sun, J.-P.; Duan, H.-S.; Meng, W.; Cameron, S.; Hill, I. G.; Yan, Y.; Mitzi, D. B. *Chem. Mater.* **2015**, *27*, 5622.

(8) Park, B. W.; Philippe, B.; Zhang, X. L.; Rensmo, H.; Boschloo, G.; Johansson, E. M. J. *Adv. Mater.* **2015**, *27*, 6806.

(9) Ogomi, Y.; Morita, A.; Tsukamoto, S.; Saitho, T.; Fujikawa, N.; Shen, Q.; Toyoda, T.; Yoshino, K.; Pandey, S. S.; Ma, T. L.; Hayase, S. *J. Phys. Chem. Lett.* **2014**, *5*, 1004.

(10) Protesescu, L.; Yakunin, S.; Bodnarchuk, M. I.; Krieg, F.; Caputo, R.; Hendon, C. H.; Yang, R. X.; Walsh, A.; Kovalenko, M. V. *Nano Lett.* **2015**, *15*, 3692.

(11) Sutton, R. J.; Eperon, G. E.; Miranda, L.; Parrott, E. S.; Kamino, B. A.; Patel, J. B.; Horantner, M. T.; Johnston, M. B.; Haghighirad, A. A.; Moore, D. T.; Snaith, H. J. *Adv. Energy Mater.* **2016**, *6*, 1502458.

(12) Hoffman, J. B.; Schleper, A. L.; Kamat, P. V. *J. Am. Chem. Soc.* **2016**, *138*, 8603.

(13) Eperon, G. E.; Paterno, G. M.; Sutton, R. J.; Zampetti, A.; Haghighirad, A. A.; Cacialli, F.; Snaith, H. J. *J. Mater. Chem. A* **2015**, *3*, 19688.

(14) Liu, F.; Zhang, Y.; Ding, C.; Kobayashi, S.; Izuishi, T.; Nakazawa, N.; Toyoda, T.; Ohta, T.; Hayase, S.; Minemoto, T.; Yoshino, K.; Dai, S.; Shen, Q. *ACS*

Nano **2017**, DOI: 10.1021/acsnano.7b05442.

(15) Tolbert, S. H.; Herhold, A. B.; Johnson, C. S.; Alivisatos, A. P. *Phys. Rev. Lett.* **1994**, *73*, 3266.

(16) Hao, F.; Stoumpos, C. C.; Cao, D. H.; Chang, R. P. H.; Kanatzidis, M. G. *Nat. Photonics* **2014**, *8*, 489.

(17) Noel, N. K.; Stranks, S. D.; Abate, A.; Wehrenfennig, C.; Guarnera, S.; Haghighirad, A. A.; Sadhanala, A.; Eperon, G. E.; Pathak, S. K.; Johnston, M. B.; Petrozza, A.; Herz, L. M.; Snaith, H. J. *Energ. Environ. Sci.* **2014**, *7*, 3061.

(18) Kumar, M. H.; Dharani, S.; Leong, W. L.; Boix, P. P.; Prabhakar, R. R.; Baikie, T.; Shi, C.; Ding, H.; Ramesh, R.; Asta, M.; Graetzel, M.; Mhaisalkar, S. G.; Mathews, N. *Adv. Mater.* **2014**, *26*, 7122.

(19) Shum, K.; Chen, Z.; Qureshi, J.; Yu, C. L.; Wang, J. J.; Pfenninger, W.; Vockic, N.; Midgley, J.; Kenney, J. T. *Appl. Phys. Lett.* **2010**, *96*, 221903.

(20) Jellicoe, T. C.; Richter, J. M.; Glass, H. F. J.; Tabachnyk, M.; Brady, R.; Dutton, S. E.; Rao, A.; Friend, R. H.; Credgington, D.; Greenham, N. C.; Bohm, M. L. *J. Am. Chem. Soc.* **2016**, *138*, 2941.

(21) Chung, I.; Song, J. H.; Im, J.; Androulakis, J.; Malliakas, C. D.; Li, H.; Freeman, A. J.; Kenney, J. T.; Kanatzidis, M. G. *J. Am. Chem. Soc.* **2012**, *134*, 8579.

(22) Chung, I.; Lee, B.; He, J. Q.; Chang, R. P. H.; Kanatzidis, M. G. *Nature* **2012**, *485*, 486.

(23) Saparov, B.; Mitzi, D. B. *Chem. Rev.* **2016**, *116*, 4558.

(24) Stoumpos, C. C.; Malliakas, C. D.; Kanatzidis, M. G. *Inorg. Chem.* **2013**, *52*, 9019.

(25) Marshall, K. P.; Walker, M.; Walton, R. I.; Hatton, R. A. *Nat. Energy* **2016**, *1*, 16178.

(26) Xu, P.; Chen, S. Y.; Xiang, H. J.; Gong, X. G.; Wei, S. H. *Chem. Mater.* **2014**, *26*, 6068.

(27) Kontos, A. G.; Kaltzoglou, A.; Siranidi, E.; Palles, D.; Angeli, G. K.; Arfanis, M. K.; Psycharis, V.; Raptis, Y. S.; Kamitsos, E. I.; Trikalitis, P. N.; Stoumpos, C. C.; Kanatzidis, M. G.; Falaras, P. *Inorg. Chem.* **2017**, *56*, 84.

(28) Xing, G. C.; Kumar, M. H.; Chong, W. K.; Liu, X. F.; Cai, Y.; Ding, H.; Asta, M.; Gratzel, M.; Mhaisalkar, S.; Mathews, N.; Sum, T. C. *Adv. Mater.* **2016**, *28*, 8191.

(29) Pan, Z.; Zhao, K.; Wang, J.; Zhang, H.; Feng, Y.; Zhong, X. *ACS Nano* **2013**, *7*, 5215.

(30) Kim, S. W.; Zimmer, J. P.; Ohnishi, S.; Tracy, J. B.; Frangioni, J. V.; Bawendi, M. G. *J. Am. Chem. Soc.* **2005**, *127*, 10526.

(31) Zhong, X. H.; Han, M. Y.; Dong, Z. L.; White, T. J.; Knoll, W. *J. Am. Chem. Soc.* **2003**, *125*, 8589.

(32) Regulacio, M. D.; Han, M. Y. *Acc. Chem. Res.* **2010**, *43*, 621.

(33) Saliba, M.; Matsui, T.; Seo, J. Y.; Domanski, K.; Correa-Baena, J. P.; Nazeeruddin, M. K.; Zakeeruddin, S. M.; Tress, W.; Abate, A.; Hagfeldt, A.; Gratzel, M. *Energ. Environ. Sci.* **2016**, *9*, 1989.

(34) Bi, D. Q.; Tress, W.; Dar, M. I.; Gao, P.; Luo, J. S.; Renevier, C.; Schenk, K.; Abate, A.; Giordano, F.; Baena, J. P. C.; Decoppet, J. D.; Zakeeruddin, S. M.; Nazeeruddin, M. K.; Gratzel, M.; Hagfeldt, A. *Sci. Adv.* **2016**, *2*, e1501170.

(35) Li, Z.; Yang, M. J.; Park, J. S.; Wei, S. H.; Berry, J. J.; Zhu, K. *Chem. Mater.* **2016**, *28*, 284.

(36) Yang, Z. B.; Rajagopal, A.; Chueh, C. C.; Jo, S. B.; Liu, B.; Zhao, T.; Jen, A. K. Y. *Adv. Mater.* **2016**, *28*, 8990.

(37) Chander, N.; Chandrasekhar, P. S.; Komarala, V. K. *RSC Adv.* **2014**, *4*, 55658.

(38) Zhong, X. H.; Feng, Y. Y.; Knoll, W.; Han, M. Y. *J. Am. Chem. Soc.* **2003**, *125*, 13559.

(39) Hao, F.; Stoumpos, C. C.; Chang, R. P. H.; Kanatzidis, M. G. *J. Am. Chem. Soc.* **2014**, *136*, 8094.

(40) Gupta, S.; Bendikov, T.; Hodes, G.; Cahen, D. *ACS Energy Lett.* **2016**, *1*, 1028.

(41) Hyun, B. R.; Zhong, Y. W.; Bartnik, A. C.; Sun, L. F.; Abruna, H. D.; Wise, F. W.; Goodreau, J. D.; Matthews, J. R.; Leslie, T. M.; Borrelli, N. F. *ACS Nano* **2008**, *2*, 2206.

(42) Urbach, F. *Phys. Rev.* **1953**, *92*, 1324.

(43) Zhang, W.; Saliba, M.; Moore, D. T.; Pathak, S. K.; Horantner, M. T.; Stergiopoulos, T.; Stranks, S. D.; Eperon, G. E.; Alexander-Webber, J. A.; Abate, A.; Sadhanala, A.; Yao, S. H.; Chen, Y. L.; Friend, R. H.; Estroff, L. A.; Wiesner, U.; Snaith, H. J. *Nat. Commun.* **2015**, *6*, 6142.

(44) De Wolf, S.; Holovsky, J.; Moon, S. J.; Loper, P.; Niesen, B.; Ledinsky, M.; Haug, F. J.; Yum, J. H.; Ballif, C. *J. Phys. Chem. Lett.* **2014**, *5*, 1035.

(45) Rai, R. C. *J. Appl. Phys.* **2013**, *113*, 153508.

(46) Tang, J.; Kemp, K. W.; Hoogland, S.; Jeong, K. S.; Liu, H.; Levina, L.; Furukawa, M.; Wang, X. H.; Debnath, R.; Cha, D. K.; Chou, K. W.; Fischer, A.; Amassian, A.; Asbury, J. B.; Sargent, E. H. *Nat. Mater.* **2011**, *10*, 765.

(47) Jeong, K. S.; Tang, J.; Liu, H.; Kim, J.; Schaefer, A. W.; Kemp, K.; Levina, L.; Wang, X. H.; Hoogland, S.; Debnath, R.; Brzozowski, L.; Sargent, E. H.; Asbury, J. B. *ACS Nano* **2012**, *6*, 89.

(48) Seruga, M.; MetikosHukovic, M.; Valla, T.; Milun, M.; Hoffschultz, H.; Wandelt, K. *J. Electroanal. Chem.* **1996**, *407*, 83.

(49) Shuttleworth, D. *J. Phys. Chem.* **1980**, *84*, 1629.

(50) Shalvoy, R. B.; Fisher, G.; Stiles, P. *Phys. Rev. B* **1977**, *15*, 1680.

(51) Liang, J.; Zhao, P.; Wang, C.; Wang, Y.; Hu, Y.; Zhu, G.; Ma, L.; Liu, J.; Jin, Z. *J. Am. Chem. Soc.* **2017**, DOI: 10.1021/jacs.7b07949.

(52) Rajendra Kumar, G.; Kim, H.-J.; Karupannan, S.; Prabakar, K. *J. Phys. Chem. C* **2017**, *121*, 16447.

(53) Chen, L.-J.; Lee, C.-R.; Chuang, Y.-J.; Wu, Z.-H.; Chen, C. *J. Phys. Chem. Lett.* **2016**, *7*, 5028.

(54) Yuan, Z.; Shu, Y.; Tian, Y.; Xin, Y.; Ma, B. *Chem. Commun.* **2015**, *51*, 16385.

(55) Liao, Y.; Liu, H.; Zhou, W.; Yang, D.; Shang, Y.; Shi, Z.; Li, B.; Jiang, X.; Zhang, L.; Quan, L. N. *J. Am. Chem. Soc.* **2017**, *139*, 6693.

(56) Smith, I. C.; Hoke, E. T.; Solis-Ibarra, D.; McGehee, M. D.; Karunadasa, H. I. *Angew. Chem., Int. Edit.* **2014**, *53*, 11232.

(57) Cao, D. H.; Stoumpos, C. C.; Farha, O. K.; Hupp, J. T.; Kanatzidis, M. G. *J. Am. Chem. Soc.* **2015**, *137*, 7843.

(58) Kagan, C. R.; Mitzi, D. B.; Dimitrakopoulos, C. D. *Science* **1999**, *286*, 945.

(59) Mitzi, D. B.; Feild, C. A.; Harrison, W. T. A.; Guloy, A. M. *Nature* **1994**, *369*, 467.

(60) Feng, H. J.; Paudel, T. R.; Tsymbal, E. Y.; Zeng, X. C. *J. Am. Chem. Soc.* **2015**, *137*, 8227.

(61) Akkerman, Q. A.; Meggiolaro, D.; Dang, Z.; De Angelis, F.; Manna, L. *ACS Energy Lett.* **2017**, *2*, 2183.

(62) Eperon, G. E.; Ginger, D. S. *ACS Energy Lett.* **2017**, *2*, 1190.

(63) Li, J. R.; Rinke, P. *Phys. Rev. B* **2016**, *94*, 045201.

(64) Supasai, T.; Rujisamphan, N.; Ullrich, K.; Chemseddine, A.; Dittrich, T. *Appl. Phys. Lett.* **2013**, *103*, 183906.

(65) Dualeh, A.; Tetreault, N.; Moehl, T.; Gao, P.; Nazeeruddin, M. K.; Gratzel, M. *Adv. Funct. Mater.* **2014**, *24*, 3250.

(66) Chen, C. Y.; Lin, H. Y.; Chiang, K. M.; Tsai, W. L.; Huang, Y. C.; Tsao, C. S.; Lin, H. W. *Adv. Mater.* **2017**, *29*, 1605290.

(67) Liu, Y. C.; Yang, Z.; Cui, D.; Ren, X. D.; Sun, J. K.; Liu, X. J.; Zhang, J. R.; Wei, Q. B.; Fan, H. B.; Yu, F. Y.; Zhang, X.; Zhao, C. M.; Liu, S. Z. *Adv. Mater.* **2015**, *27*, 5176.

(68) Zhang, Y. H.; Ding, C.; Wu, G. H.; Nakazawa, N.; Chang, J.; Ogomi, Y.; Toyoda, T.; Hayase, S.; KatayamA, K.; Shen, Q. *J. Phys. Chem. C* **2016**, *120*, 28509.

(69) Shen, Q.; Ogomi, Y.; Das, S. K.; Pandey, S. S.; Yoshino, K.; Katayama, K.; Momose, H.; Toyoda, T.; Hayase, S. *Phys. Chem. Chem. Phys.* **2013**, *15*, 14370.

(70) Shen, Q.; Ogomi, Y.; Chang, J.; Tsukamoto, S.; Kukihara, K.; Oshima, T.; Osada, N.; Yoshino, K.; Katayama, K.; Toyoda, T.; Hayase, S. *Phys. Chem. Chem. Phys.* **2014**, *16*, 19984.

(71) Ono, M.; Nishihara, T.; Ihara, T.; Kikuchi, M.; Tanaka, A.; Suzuki, M.; Kanemitsu, Y. *Chem. Sci.* **2014**, *5*, 2696.

(72) Gimenez, S.; Mora-Sero, I.; Macor, L.; Guijarro, N.; Lana-Villarreal, T.; Gomez, R.; Diguna, L. J.; Shen, Q.; Toyoda, T.; Bisquert, J. *Nanotechnology* **2009**, *20*, 295204.

(73) Ruhle, S.; Shalom, M.; Zaban, A. *ChemPhysChem* **2010**, *11*, 2290.

(74) Lin, S. C.; Lee, Y. L.; Chang, C. H.; Shen, Y. J.; Yang, Y. M. *Appl. Phys. Lett.* **2007**, *90*, 143517.

(75) Pan, Z. X.; Zhang, H.; Cheng, K.; Hou, Y. M.; Hua, J. L.; Zhong, X. H. *ACS Nano* **2012**, *6*, 3982.

(76) Du, J.; Du, Z. L.; Hu, J. S.; Pan, Z. X.; Shen, Q.; Sung, J. K.; Long, D. H.; Dong, H.; Sun, L. T.; Zhong, X. H.; Wan, L. J. *J. Am. Chem. Soc.* **2016**, *138*, 4201.

(77) Pernik, D. R.; Tvrdy, K.; Radich, J. G.; Kamat, P. V. *J. Phys. Chem. C* **2011**, *115*, 13511.

(78) Jumabekov, A. N.; Deschler, F.; Bohm, D.; Peter, L. M.; Feldmann, J.; Bein, T. *J. Phys. Chem. C* **2014**, *118*, 5142.

(79) Liu, F.; Zhu, J.; Wei, J. F.; Li, Y.; Hu, L. H.; Huang, Y.; Takuya, O.; Shen, Q.; Toyoda, T.; Zhang, B.; Yao, J. X.; Dai, S. Y. *J. Phys. Chem. C* **2014**, *118*, 214.

(80) Guijarro, N.; Lana-Villarreal, T.; Mora-Seró, I.; Bisquert, J.; Gómez, R. *J. Phys. Chem. C* **2009**, *113*, 4208.

(81) Plass, R.; Pelet, S.; Krueger, J.; Gratzel, M.; Bach, U. *J. Phys. Chem. B* **2002**, *106*, 7578.

(82) Wu, K. F.; Liang, G. J.; Shane, Q. Y.; Ren, Y. P.; Kong, D. G.; Lian, T. Q. *J. Am. Chem. Soc.* **2015**, *137*, 12792.

(83) González-Pedro, V.; Xu, X.; Mora-Seró, I.; Bisquert, J. *ACS Nano* **2010**, *4*, 5783.

(84) Santra, P. K.; Kamat, P. V. *J. Am. Chem. Soc.* **2012**, *134*, 2508.

(85) Mora-Seró, I.; Giménez, S.; Fabregat-Santiago, F.; Gómez, R.; Shen, Q.; Toyoda, T.; Bisquert, J. *Acc. Chem. Res.* **2009**, *42*, 1848.

(86) Kojima, A.; Teshima, K.; Shirai, Y.; Miyasaka, T. *J. Am. Chem. Soc.* **2009**, *131*, 6050.

(87) Tao, L.; Huo, Z.; Ding, Y.; Li, Y.; Dai, S.; Wang, L.; Zhu, J.; Pan, X.; Zhang, B.; Yao, J. *J. Mater. Chem. A* **2015**, *3*, 2344.

(88) Tao, L.; Huo, Z.; Dai, S.; Ding, Y.; Zhu, J.; Zhang, C.; Zhang, B.; Yao, J.; Nazeeruddin, M. K.; Grätzel, M. *J. Phys. Chem. C* **2014**, *118*, 16718.

(89) Heo, J. H.; Jang, M. H.; Lee, M. H.; You, M. S.; Kim, S.-W.; Lee, J.-J.; Im, S. H. *RSC Adv.* **2017**, *7*, 3072.

(90) Chang, J. A.; Rhee, J. H.; Im, S. H.; Lee, Y. H.; Kim, H.-j.; Seok, S. I.; Nazeeruddin, M. K.; Gratzel, M. *Nano Lett.* **2010**, *10*, 2609.

(91) Im, S. H.; Lim, C.-S.; Chang, J. A.; Lee, Y. H.; Maiti, N.; Kim, H.-J.; Nazeeruddin, M. K.; Grätzel, M.; Seok, S. I. *Nano Lett.* **2011**, *11*, 4789.

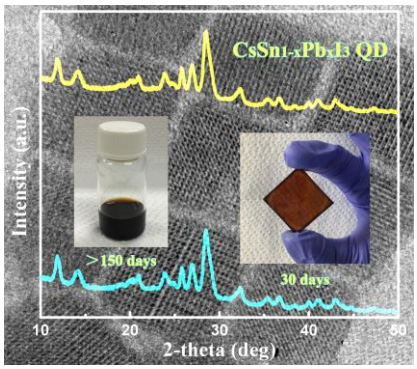

TOC